

Function of 7,7,8,8-tetracyanoquinodimethane (TCNQ) on electrocatalytic hydrogen generation catalyzed by N,N'-benzene bis (salicylidiminato)nickel(II)



Dan Xue^a, Qi-Ying Lv^b, Chen-Neng Lin^a, Shu-Zhong Zhan^{a,*}

^a College of Chemistry and Chemical Engineering, South China University of Technology, Guangzhou 510640, China

^b School of Chemistry & Chemical Engineering, Huazhong University of Science and Technology, Wuhan 430074, China

ARTICLE INFO

Article history:

Received 9 March 2016

Accepted 25 May 2016

Available online 5 June 2016

Keywords:

Nickel(II) complex

TCNQ

Molecular electrocatalyst

Water reduction

Hydrogen evolution

ABSTRACT

In the presence of trimethylamine, the reaction of N,N'-benzene bis(salicylidimine) (H₂L) with NiCl₂·6H₂O affords a nickel(II) complex, [NiL] (**1**), and the reaction of H₂L with NiCl₂·6H₂O and TCNQ provides a TCNQ compound, [LNi(TCNQ)] (**2**). Electrochemical studies show that **1** electrocatalyzes hydrogen evolution, both from acetic acid with a turnover frequency (TOF) of 53.25 moles of hydrogen per mole of catalyst per hour at an overpotential (OP) of 941.6 mV (in DMF), and from an aqueous buffer solution (pH 7.0) with a TOF of 462.33 moles of hydrogen per mole of catalyst per hour at an OP of 836.7 mV. **2** can electrocatalyze hydrogen evolution, both from acetic acid with a TOF of 62.56 moles of hydrogen per mole of catalyst per hour at an OP of 941.6 mV (in DMF), and from an aqueous buffer solution (pH 7.0) with a TOF of 909.58 moles of hydrogen per mole of catalyst per hour at an OP of 836.7 mV. To testify that TCNQ plays a vital role in determining the catalytic activities of the nickel complex, we have systematically studied the electrocatalytic activities of **1** and **2**, to provide a possible catalytic mechanism for hydrogen generation by the nickel complexes. This observation suggests that the presence of TCNQ is a key structural feature for eliciting proton or water reduction catalysis. This can be attributed to negatively charged TCNQ, formed from **2**, that can stabilize the low oxidation state of the nickel ion.

© 2016 Elsevier Ltd. All rights reserved.

1. Introduction

Hydrogen is one of the most ideal sources for energy in the future, because of its numerous advantages such as recyclability and pollution-free use [1–3]. Water is the only waste-free electron-source substrate that could sustain the scale of the process required to supply our energy demands. Thus water splitting is an important and simple method for hydrogen production with high purity and in large quantities [4]. The generation of hydrogen by electrochemical reduction of a proton source, such as water, represents an attractive approach for storing the electrical energy transiently produced by renewable energy sources [5,6]. To increase the reaction rate, it is necessary to use an efficient hydrogen evolution reaction electrocatalyst. Therefore, many research groups, including ours, have designed molecular catalysts by employing abundant metals, and several complexes of nickel [7,8], cobalt [9–13], copper [14–17] and molybdenum [18,19] have

been developed as electrocatalysts for the reduction of protons or water to form H₂. Despite much progress in water reduction catalysis, major improvements in several areas, including lowering overpotentials, increasing catalyst durability and using earth-abundant elements, are needed before efficient electrocatalytic water reduction can be realized. Especially, structural complexity, insolubility in aqueous media and low pH conditions severely limit their practical utility [20].

Our interest focuses on the design of molecular electrocatalysts that are water soluble and can efficiently catalyze water reduction. To the best of our knowledge, there is as yet no report on electrochemical water reduction by TCNQ compounds. As we know, TCNQ is electron poor and forms numerous donor–acceptor compounds [21], where radical anions are stabilized by charge and spin delocalization, forming numerous stable electron transfer salts. Generally, compounds containing TCNQ exhibit metal-like electrical conductivity [22] and ferromagnetic ordering [23]. Reported here is an electrocatalyst based on one nickel–TCNQ complex, [LNi(TCNQ)] (**2**), for hydrogen evolution from both acetic acid and aqueous buffer solution, as well as the effect of TCNQ on the catalytic properties of the nickel(II) complex. We hope this can

* Corresponding author.

E-mail address: shzhzhan@scut.edu.cn (S.-Z. Zhan).

establish a new method for the improvement in electrocatalytic hydrogen production by structural modification of the catalyst.

2. Experimental section

2.1. Materials and physical measurements

The nickel complex [LNi] (**1**) was prepared by using the literature procedure [24]. Elemental analyses for C, H and N were obtained on a Perkin-Elmer analyzer model 240. An ESI-MS experiment was performed on a Bruker Daltonics Esquire 3000 spectrometer by introducing samples directly into the ESI source using a syringe pump. IR spectra were directly obtained as KBr pellets on a Bruker 1600 FT-IR spectrometer from 4000 to 400 cm^{-1} . Electronic spectra were recorded on a Lambda-900 spectrophotometer. Cyclic voltammograms were obtained on a CHI-660E electrochemical analyzer under N_2 using a three-electrode cell in which a glassy carbon electrode was the working electrode, an Ag/AgNO₃ or saturated Ag/AgCl electrode was the reference electrode and a platinum wire was the auxiliary electrode. In organic media, the ferrocene/ferrocenium (1+) couple was used as an internal standard and a solution of 0.10 M [(n-Bu)₄N]ClO₄ was used as the supporting electrolyte. Controlled-potential electrolysis (CPE) in DMF was conducted using an air-tight glass double compartment cell separated by a glass frit. The working compartment was fitted with a glassy carbon plate and an Ag/AgNO₃ reference electrode. The auxiliary compartment was fitted with a Pt gauze electrode. The working compartment was filled with 50 mL of 0.10 M [(n-Bu)₄N]ClO₄ DMF solution with acetic acid, while the auxiliary compartment was filled with 35 mL of 0.10 M [(n-Bu)₄N]ClO₄ DMF solution, resulting in equal solution levels in both compartments. Both compartments were purged for 1 h with N_2 and cyclic voltammograms (CVs) were recorded as controls. Controlled-potential electrolysis (CPE) in aqueous media was conducted using an air-tight glass double compartment cell separated by a glass frit. The working compartment was fitted with a glassy carbon plate and an Ag/AgCl reference electrode. The auxiliary compartment was fitted with a Pt gauze electrode. The working compartment was filled with 50 mL of 0.25 M buffer, while the auxiliary compartment was filled with 35 mL phosphate buffer solution. Adding nickel complexes, both compartments were purged for 1.5 h with nitrogen and CVs were recorded as controls. After electrolysis, a 0.5 mL aliquot of the headspace was removed and replaced with 0.5 mL of CH_4 . The headspace sample was injected into the gas chromatograph (GC). GC experiments were carried out with an Agilent Technologies 7890A gas chromatography instrument.

2.2. Synthesis of [LNi] (**1**)

To a solution of o-phenylenediamine (1.08 g, 10 mmol) in methanol (20 ml), salicylaldehyde (2.45 g, 20 mmol) was added, and the mixture was refluxed for 8 h. To the above yellow mixture was added triethylamine (2.00 g, 20 mmol) and NiCl₂·6H₂O (2.34 g, 10 mmol) with stirring for 20 min, the color of the solution changed from yellow to brown. On slow evaporation at room temperature for several days, brown crystals appeared. The crystals were collected and dried in *vacuo* (3.15 g, 85%). *Anal.* Calc. for C₂₀H₁₄N₂NiO₂: C, 64.75; H, 3.26; N, 7.55%. Found: 64.86; H, 3.76; N, 7.54%.

2.3. Synthesis of [LNi(TCNQ)] (**2**)

A solution of o-phenylenediamine (0.54 g, 5.0 mmol) and salicylaldehyde (1.23 g, 10.0 mmol) in 50 ml methanol was refluxed with stirring for 8 h, whereupon a yellow powder was obtained. To the above yellow mixture was added triethylamine (1.00 g,

10.0 mmol), NiCl₂·6H₂O (1.17 g, 5.0 mmol) and TCNQ (1.02 g, 5.0 mmol) in 50 ml CH₂Cl₂ with stirring. The color of the solution changed from yellow to deep-green, and it was allowed to react for 3 h at room temperature, and then it was filtered. On slow evaporation at room temperature for several days, deep green crystals appeared. The crystals were collected and dried in *vacuo* (1.26 g, 43.8% based on TCNQ). *Anal.* Calc. for C₃₂H₁₈N₆NiO₂: C, 66.82; H, 2.80; N, 14.61. Found: 66.86; H, 2.79; N, 14.64%. IR band (KBr pellets, cm^{-1}) ν : 2217.

2.4. Crystal structure determination

X-ray analysis of the complex [LNi(TCNQ)] (**2**) was carried out with a Bruker Smart Apex II DUO area detector using graphite monochromated Mo K α radiation ($\lambda = 0.71073 \text{ \AA}$) at room temperature. All empirical absorption corrections were applied using the SADABS program [25]. The structure was solved using direct methods and the corresponding non-hydrogen atoms were refined anisotropically. All the hydrogen atoms of the ligands were placed in calculated positions with fixed isotropic thermal parameters and included in the structure factor calculations in the final stage of the full-matrix least-squares refinement. All calculations were performed using the SHELXTL computer program [26]. Crystallographic data for complex **2** are given in Table 1 and selected bond lengths and angles are listed in Table 2.

3. Results and discussion

3.1. Synthesis and characterization of the nickel complexes [LNi] (**1**) and [LNi(TCNQ)]·MeOH (**2**·MeOH)

Typically, the reaction of the TCNQ molecule with transition metal centers leads to di-, tri- or tetranuclear nitrile-bonded σ compounds, to π compounds with side-on coordination, or to the corresponding ion pair compounds without direct coordination [27–31]. However, when the Ni^{II} complex NiL was used as a metal source to react with TCNQ, an unprecedented TCNQ-compound **2** (Scheme 1) resulted, which is soluble in both aqueous media ($1.5 \times 10^{-3} \text{ mol L}^{-1}$) and general organic solvents, such as CH₃OH and CH₃CN, etc. The infrared spectrum of **2** shows one peak at 2217 cm^{-1} , which is assigned to the ν_{CN} band of the TCNQ molecule of **2** (Fig. S1), indicating that the four cyano groups are in the same state.

Table 1

Crystallographic data for [LNi(TCNQ)]·MeOH (**2**·MeOH).

Empirical formula	C ₃₃ H ₂₂ N ₆ O ₃ Ni
Formula weight	609.27
λ (Å)	0.71073
Crystal system	triclinic
Space group	P $\bar{1}$
Volume (Å ³)	1382.61(13)
<i>a</i> (Å)	11.2467(7)
<i>b</i> (Å)	11.6531(5)
<i>c</i> (Å)	11.7725(6)
α (°)	73.1900(10)
β (°)	69.628(2)
γ (°)	81.457(2)
<i>Z</i>	2
Dc (Mg m ⁻³)	1.464
F(000)	628
θ range for data collection	6.252–50.052
Data/restraints/parameters	4873/0/390
Goodness-of-fit (GOF) on F^2	1.091
Final <i>R</i> indices [$I > 2\sigma(I)$]	<i>R</i> 1 = 0.0342, <i>wR</i> 2 = 0.0718
<i>R</i> indices (all data)	<i>R</i> 1 = 0.0728, <i>wR</i> 2 = 0.0875

Table 2
The selected bond lengths (Å) and angles (°) for [LNi(TCNQ)]·MeOH (**2**·MeOH).

Ni1–O1	1.8444(16)	Ni1–O2	1.8391(19)
Ni1–N5	1.851(2)	Ni1–N6	1.8526(19)
C24–C25	1.440(4)	C25–C26	1.338(4)
C24–C28	1.369(4)	C28–C31	1.431(4)
N1–C29	1.346(4)	N2–C30	1.140(3)
N3–C31	1.139(3)	N4–C32	1.128(3)
O2–Ni1–N6	95.45(9)	O2–Ni1–O1	83.58(8)
O2–Ni1–N5	178.59(9)	O1–Ni1–N6	178.18(9)
O1–Ni1–N5	95.14(8)	N5–Ni1–N6	85.85(9)

Complex **2**·MeOH crystallizes in the triclinic system, space group $P\bar{1}$ with two formula units present per unit cell. As shown in Fig. 1 (top), the X-ray analysis reveals that the crystal structure of **2**·MeOH consists of one Ni(II) complex [NiL], one TCNQ molecule and one methanol molecule. In the [NiL] unit, the central nickel atom is coordinated by two oxygen atoms and two nitrogen atoms of the ligand (L^{2-}) in a distorted square geometry. The Ni–O bond lengths fall in the range 1.8391(19)–1.8444(16) Å, and the O–Ni–O angle is 83.58(8)°. The Ni–N bond lengths are 1.851(2) and 1.8526(19) Å, and the N–Ni–N angle is 85.85(9)°. In the three-dimensional packing arrangement, the [NiL] unit and TCNQ molecule lie in the same plane (Fig. 1 (bottom)).

The C≡N bond lengths of TCNQ in **2**·MeOH range from 1.128(3) to 1.14(3) Å, and the average length (1.136 Å) is similar to free TCNQ (1.140 Å) [32]. To test the degree of charge transfer between the TCNQ molecule and [LNi], Kistenmacher's equation was used: the relationship $\rho = A[c/(b+d)] + B$ ($A = -41.667$, $B = 19.833$) was determined from neutral TCNQ ($\rho = 0$) [33] and [Ni([14]aneN₄)](TCNQ)₂ ($\rho = -1.0005$) [34], where c , b and d are the TCNQ bond lengths. The charge of the TCNQ group in complex **2** was estimated from Kistenmacher relationship as $\rho = -0.061$ (Scheme 2 and Table 3), suggesting that TCNQ is in the neutral state.

As shown in Fig. S4a, the absorption spectrum of compound **2** exhibits two peaks at 420 (the $\pi \rightarrow \pi^*$ transition of the ring in TCNQ) and 740 nm (a charge-transfer involving radical anions (TCNQ/TCNQ⁻), which were found in the free TCNQ [35,36] (Fig. S4b).

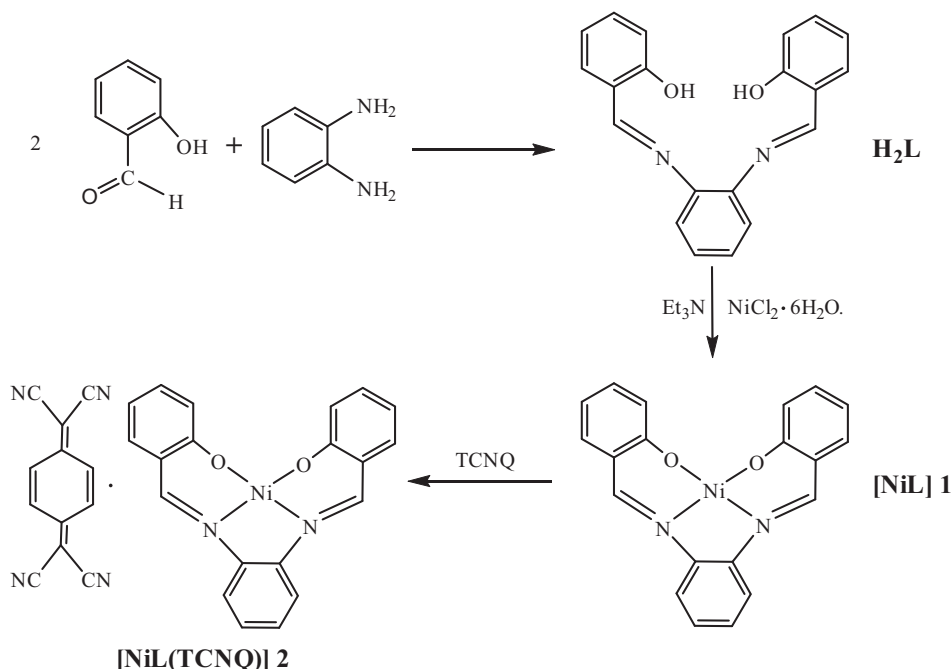
3.2. Electrochemical studies

To study the electrochemical properties of TCNQ, **1** and **2**, cyclic voltammograms (CVs) were conducted in DMF solution with 0.10 M [(n-Bu)₄N]ClO₄ as the supporting electrolyte. Fig. 2a represents the CV of TCNQ in DMF. The first reduction potential of TCNQ is presumably at 0.278 V, and two typical reversible redox peaks for TCNQ are found at the potentials -0.315 and 0.278 V versus Ag/AgNO₃, respectively. Complex **1** shows a quasi-reversible redox couple at -1.41 V versus Ag/AgNO₃, which can be assigned to that of Ni^{II}/Ni^I (Fig. 2b). Compared to TCNQ, the TCNQ-nickel complex **2** displays two reversible redox couples at -0.30 and 0.275 V versus Ag/AgNO₃, which are assigned to those of TCNQ, and a quasi-reversible Ni^{III}/Ni^{II} redox couple at -1.39 V versus Ag/AgNO₃ (Fig. 2c). Note, the potential of Ni^{III} is shifted by 0.02 V as a result of the introduction of TCNQ. From Fig. S5, all the current responses of the redox events at -0.37 V for TCNQ, -1.46 V for **1** and -1.41 V for **2** show a linear dependence on the square root of the scan rate, indicative of a diffusion-controlled process, with the electrochemically active species freely diffusing in solution.

To investigate the effect of the temperature of the media on the electrochemical behaviors of TCNQ and the nickel complexes, CVs were measured in the range 298–328 K. For **1**, the current strength significantly increases near -1.46 V on increasing the temperature from 298 to 328 K (Fig. S6a). Note, both current strengths increase near -1.4 and -0.37 V with increasing temperature from 298 to 328 K for **2** (Fig. S6b). Similar to **2**, the current strength for TCNQ also increases at -0.37 V with increasing temperature from 298 to 328 K, and the potential of TCNQ/TCNQ⁻ moves negative by about 40 mV from -0.37 to -0.41 V (Fig. S6c).

3.3. Catalytic hydrogen evolution from acetic acid in DMF

From Fig. 3a, it can be seen that the catalytic currents near -1.48 V increase with increasing proton concentration (the acetic acid concentration was increased from 0.0 to 22.80 mM). This indicates that hydrogen evolution electrocatalyzed by **1** requires the reduction of Ni(II) to Ni(I) and protonation. Interestingly, when the acetic acid concentration increases from 0.0 to 22.80 mM



Scheme 1. Synthesis of the nickel complexes [LNi] **1** and [LNi(TCNQ)] **2**.

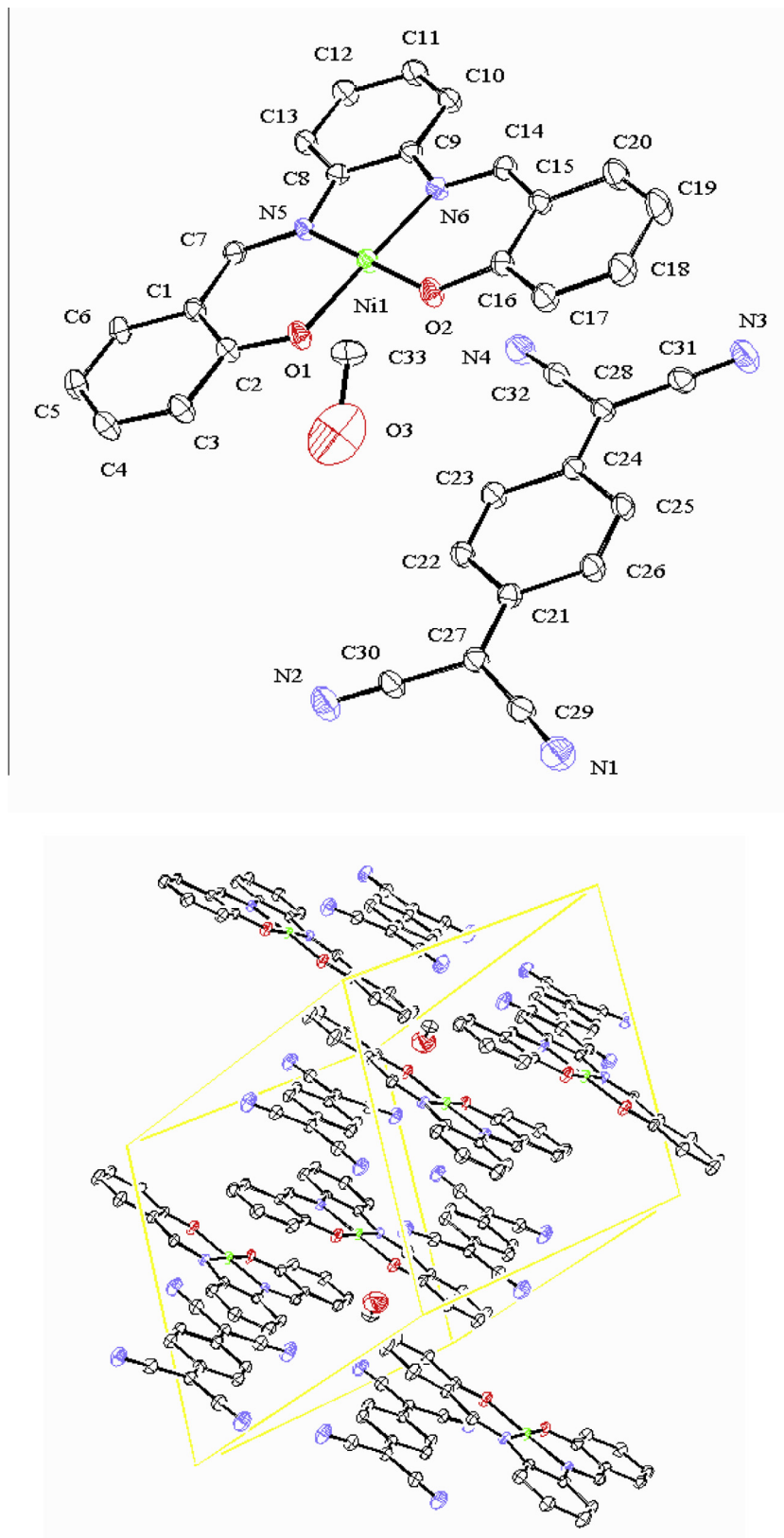
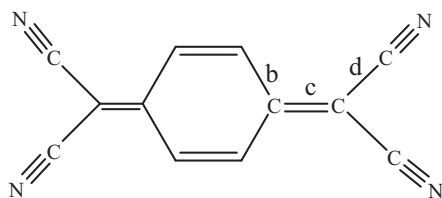


Fig. 1. ORTEP drawing of complex **2** with thermal ellipsoids at the 50% probability level (hydrogen atoms are not shown) (top); Molecular packing arrangement of **2** (bottom).

(Fig. 3a), the potential of $\text{Ni}^{\text{II}}/\text{Ni}^{\text{I}}$ becomes more positive by about 50 mV, from -1.48 to -1.43 V, and the onset of the catalytic wave also becomes more positive by about 430 mV compared to that in the absence of **1**. For **2**, the catalytic current near -1.45 V also

increases with an increasing proton concentration (the acetic acid concentration was increased from 0.0 to 22.80 mM) (Fig. 3b), and the potential of $\text{Ni}^{\text{II}}/\text{Ni}^{\text{I}}$ becomes slightly more negative by about 9 mV, from -1.456 to -1.465 V. Interestingly, when the acetic acid



Scheme 2. Schematic representation of 7,7,8,8-tetracyanoquinodimethane.

Table 3
Important structural features in several TCNQ complexes.

Compounds	Bond distances (Å)			References
	b	c	d	
TCNQ	1.448(4)	1.374(3)	1.441(4)	[30]
[Ni(N ₄ cisdiene)](TCNQ) ₂	1.410	1.410	1.400	[31]
[LNi(TCNQ)] 2	1.433(5)	1.365(5)	1.431(5)	this work

concentration increases from 0.0 to 22.80 mM (Fig. 2b), the onset of the catalytic wave moves to a higher potential from -1.28 to -1.24 V versus Ag/AgNO₃. For TCNQ, the catalytic current near -0.45 V remains almost constant with increasing proton concentration (the acetic acid concentration was increased from 0.0 to 22.80 mM) (Fig. 3c), indicating that TCNQ does not have activity for proton reduction. Thus, the introduction of **1** to TCNQ is essential for catalytic activity.

To testify that TCNQ plays a vital role in determining the catalytic activity of the nickel complex, bulk electrolysis of **1** and **2** were conducted in DMF solutions with acetic acid at variable applied potentials using a glassy carbon plate electrode in a double-compartment cell. Fig. 4 shows the total charges of bulk electrolysis of **1** and **2** in the presence of acid, and the charge significantly increased when the applied potential was more negative. When the applied potential was -1.45 V versus Ag/AgNO₃, the maximum charge reached 98 and 115 mC during 2 min of electrolysis, respectively (Fig. 4a and b). A CPE experiment under the same potential without **1** or **2** gave a charge of only 6 mC (Fig. 4c), showing that the nickel complexes do indeed serve as effective hydrogen producers under such conditions. Assuming every catalyst molecule was distributed only on the electrode surface and every electron was used for the reduction of protons, according to Eqs. (1) [13] and (2) [37], we calculated the TOF for the catalysts as reaching a maximum of 53.25 for **1** and 62.56 for 2 moles of hydrogen per mole of catalyst per hour at an overpotential of 941.6 mV, respectively (Eqs. (S1) and (S2)). Remarkably, **2** exhibits more activity than **1**, indicating that the introduction of TCNQ into **1** is essential for more efficient activity. These results also suggest that the nickel complexes with more positive Ni^{II/I} redox potentials show a higher activity for hydrogen generation, which is different from the reported results [38].

$$\text{TOF} = \Delta C / (F^* n_1^* n_2^* t) \quad (1)$$

$$\begin{aligned} \text{Overpotential} &= \text{Applied potential} - E_{\text{HA}}^{\ominus} \\ &= \text{Applied potential} - (E_{\text{H}^+}^{\ominus} - (2.303RT/F)pK_{\text{aHA}}) \end{aligned} \quad (2)$$

where ΔC is the charge from the catalyst solution during CPE minus the charge from solution without catalyst during CPE; F is Faraday's constant, n_1 is the number of moles of electrons required to generate one mole of H₂, n_2 is the number of moles of catalyst in solution, and t is the duration of the electrolysis.

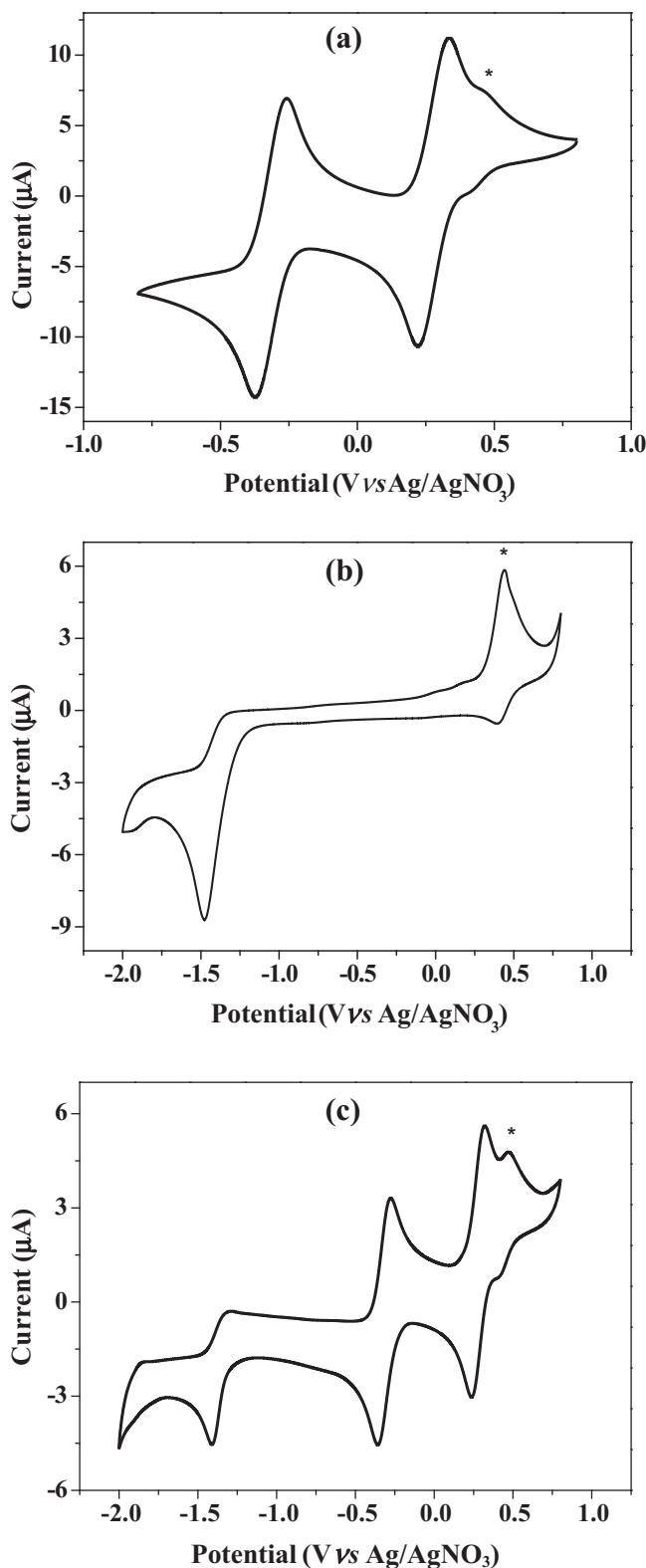


Fig. 2. Cyclic voltammograms of 2.33 mM TCNQ (a), 2.33 mM [LNi] (**1**) (b) and 1.86 mM [LNi(TCNQ)] (**2**) (c). Conditions: room temperature, 0.10 M [n-Bu₄N]ClO₄ as the supporting electrolyte, glassy carbon working electrode (1 mm diameter), Pt counter electrode, Ag/AgNO₃ reference electrode, scan rate 0.10 V/s, ferrocene internal standard (*).

Generally, hydrogen evolution reactions occur via metal-hydride species, which have been demonstrated in several catalytic systems, such as diiron mimics of iron-only hydrogenases

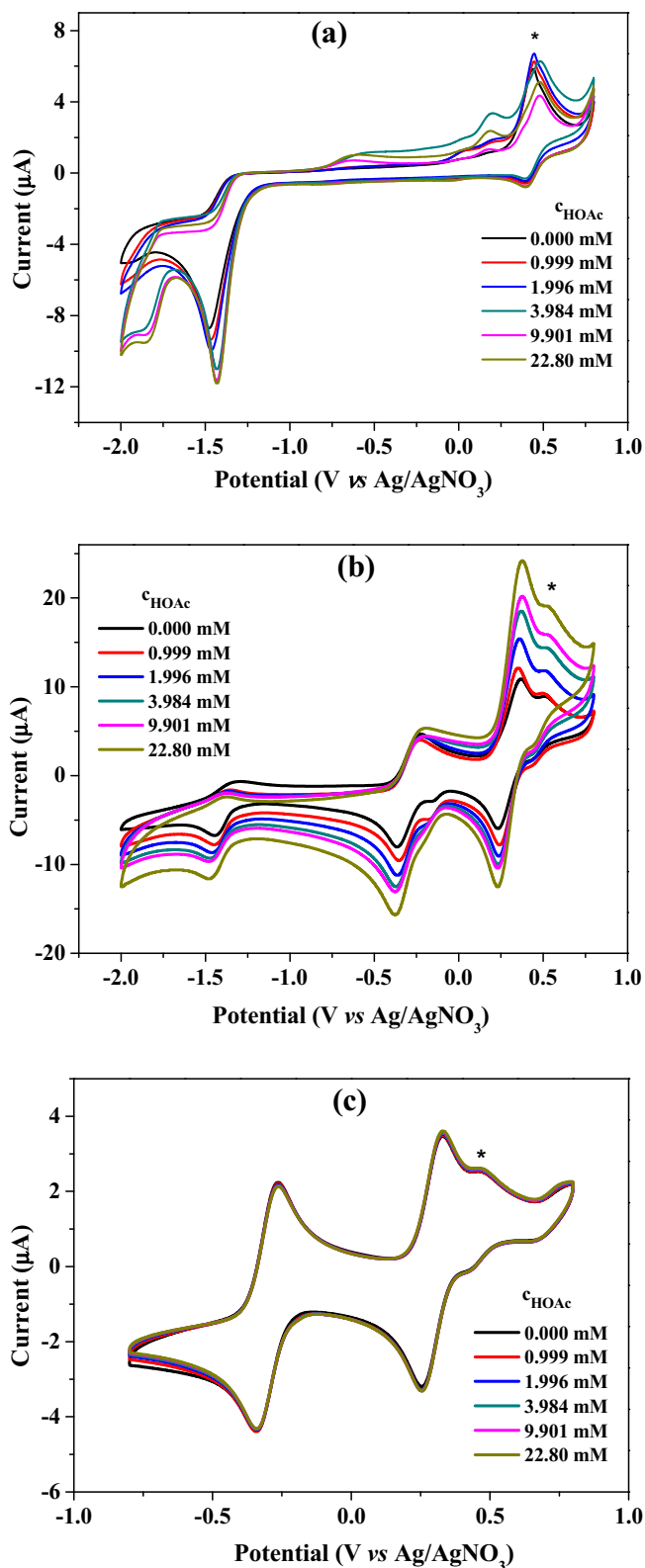


Fig. 3. Cyclic voltammograms of a 2.23 mM solution of [NiL] (**1**) (a), a 2.23 mM solution of [LNi(TCNQ)] (**2**) (b) and a 2.23 mM solution of TCNQ (**c**), with varying concentrations of acetic acid in DMF. Conditions: 0.10 M [n-Bu₄N]ClO₄ as the supporting electrolyte, scan rate: 0.10 V/s, glassy carbon working electrode (1 mm diameter), Pt counter electrode, Ag/AgNO₃ reference electrode, ferrocene internal standard (*).

[3,39,40], molecular nickel catalysts [Ni(P^{ph}N₂^{CGH4X})₂](BF₄)₂ (P^{ph}N₂^{CGH4X} = 1,5-di(para-X-phenyl)-3,7-diphenyl-1,5-diphosphy-

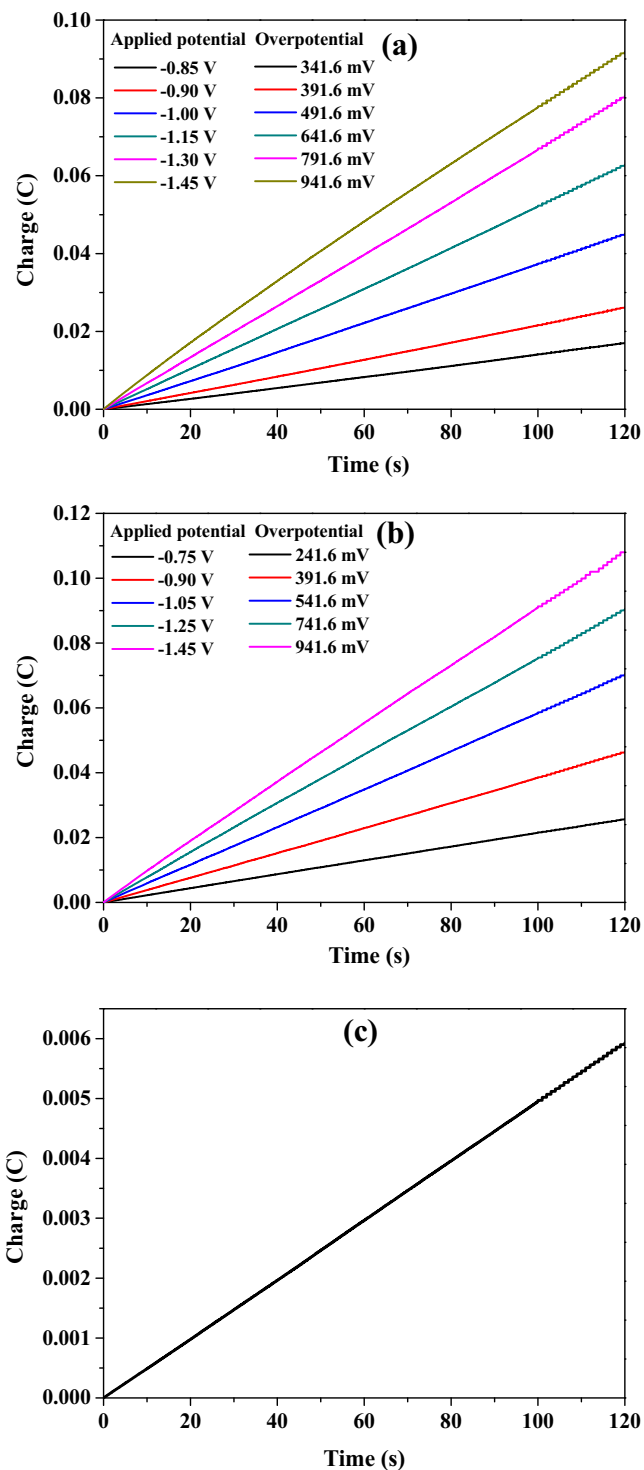


Fig. 4. Charge build-up versus time from electrolysis of 0.10 M [n-Bu₄N]ClO₄ with 5.36 μM complex **1** (a), 5.36 μM complex **2** (b) and 2.0 mM acetic acid in DMF under various applied potentials. All data have been deducted blank. (c) Charge build-up versus time from electrolysis of 0.10 M [n-Bu₄N]ClO₄ in DMF at -1.45 V versus Ag/AgNO₃.

cloctane; X = OMe, Me, CH₂P(O)(OEt)₂, Br, CF₃) [41], cobalt macrocyclic complexes [3] and [Co(dmgBF₂)₂L] (dmg²⁻ = the dimethylglyoximate dianion; L = CH₃CN or N,N'-dimethylformamide) [42]. Based on the above analyses, we propose a presumed mechanism depicted in Scheme 3 for the generation of hydrogen from acetic acid mediated by **1**. One-electron reduction of [LNi^{II}] gives a putative [LNi^I]⁻ species. Addition of a hydrogen proton yields the [LNi^I-H]

species, a highly reactive intermediate. Further one-electron reduction of the $[\text{LNi}^{\text{II}}\text{-H}]$ species affords H_2 and regenerates the starting $[\text{LNi}^{\text{II}}]$. In order to confirm these results, we also tried to apply H_2L only as a catalyst for hydrogen generation (Fig. S7). Obviously, there was no catalyst effect for hydrogen generation when compared to $[\text{LNi}]$ (1). Although the relative contributions are indistinguishable in this analysis, we suspect that these processes are complementary H_2 evolution pathways.

3.4. Catalytic hydrogen evolution in aqueous media

We further explored the electrochemical behaviors of $[\text{LNi}]$ (1) and $[\text{LNi}(\text{TCNQ})]$ (2) in buffered aqueous solutions at varying pHs, where $\text{pH} = 4.5\text{--}7.0$, which is the range associated with catalytic water reduction, a much more attractive medium for the sustainable generation of hydrogen. As shown in Fig. 5a, in the absence of 1, a catalytic current was not apparent until a potential of -1.48 V versus Ag/AgCl was attained. Upon addition of complex 1, the onset of the catalytic current was observed at about -1.25 V versus Ag/AgCl , showing that addition of complex 1 can reduce the potential, and the current strength increased with increasing concentrations of 1 from 0.580 to $2.319\text{ }\mu\text{M}$ (Fig. 5a). From Fig. 5b, the onset of this catalytic current is clearly influenced by the solution pH, the applied potential declined with increasing pH, evidencing the involvement of a proton in the initial stage of the electrochemical catalysis. From Fig. 6a, with addition of 2, the onset of the catalytic current was observed at about -1.05 V versus Ag/AgCl , and the current strength increased significantly with increasing concentration of 2 from 0.580 to $2.319\text{ }\mu\text{M}$ (Fig. 6a). From Fig. 6b, 2 shows a pH-dependent peak, which is responsible for the catalytic water reduction, and the applied potential declined with increasing pH.

To further confirm that TCNQ plays a vital role in hydrogen production catalyzed by the nickel complex in aqueous media, bulk electrolysis was measured in a 0.25 M aqueous buffer solution ($\text{pH} 7.0$) containing 1 or 2. When the applied potential was -1.45 V versus Ag/AgCl , the maximum charge was only 23 mC for 2 min of electrolysis in the absence of complex 1 (Fig. 7a). Under the same conditions, the charge reached 822 mC during 2 min of electrolysis in the presence of 1 (Fig. 7b), accompanied by evolution of a gas, which was confirmed as H_2 by gas

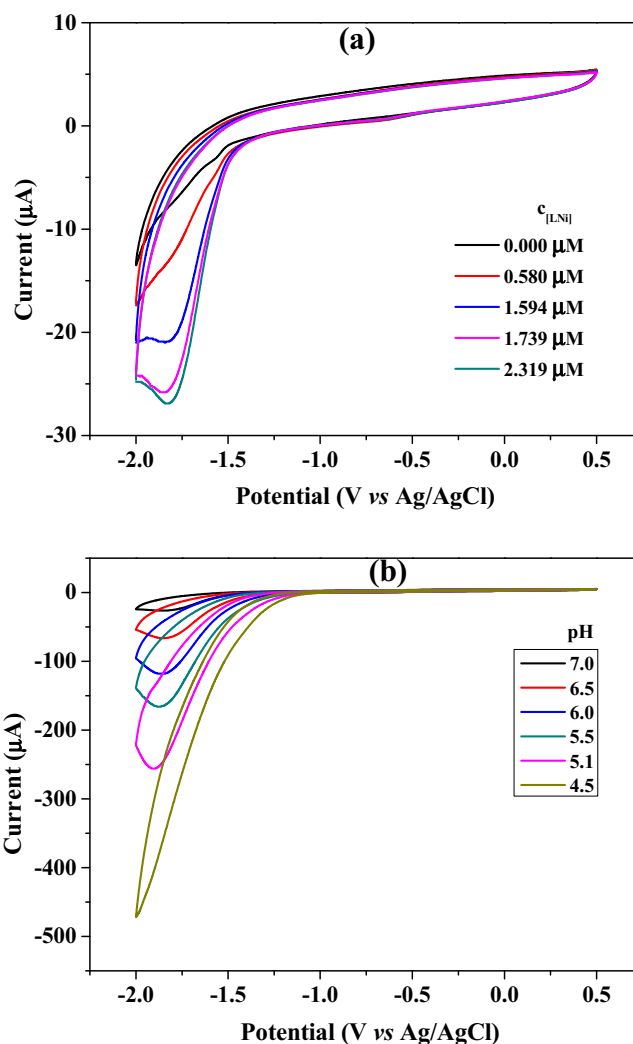
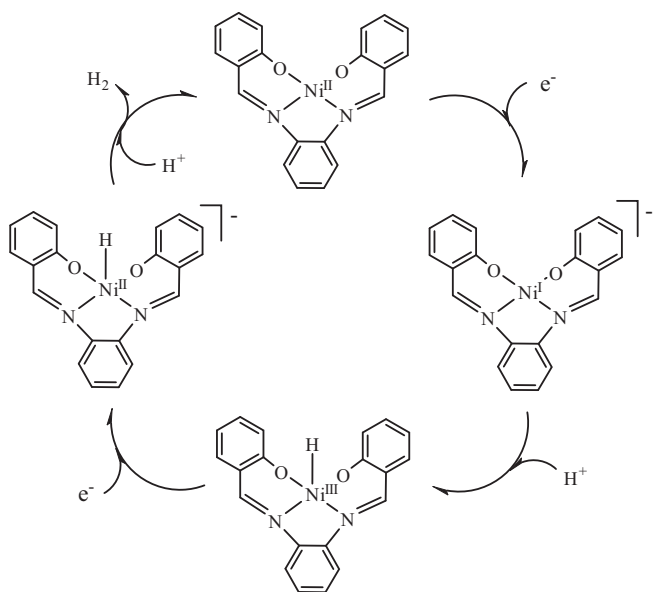


Fig. 5. (a) Cyclic voltammograms of complex 1 at different concentrations. (b) Cyclic voltammograms of complex 1 ($0.232\text{ }\mu\text{M}$) at different pH values. Conditions: 0.25 M phosphate buffered solution ($\text{pH} 7.0$), glassy carbon working electrode (1 mm diameter), Pt wire counter electrode, Ag/AgCl reference electrode.

chromatography. According to Fig. S8a, $\sim 7.25\text{ mL}$ of H_2 was produced over an electrolysis period of 1 h with a Faradaic efficiency of 96.53% for H_2 (Fig. S8-b). According to Eqs. (1) and (3) [9,43], we calculated the TOF for the catalyst as reaching a maximum of 462.33 moles of hydrogen per mole of catalyst per hour at an overpotential of 837.6 mV (Eq. (S3)), where

$$\begin{aligned} \text{Overpotential} &= \text{Applied potential} - E(\text{pH}) \\ &= \text{Applied potential} - (-0.059\text{pH}) \end{aligned} \quad (3)$$

Fig. 7c shows the total charge of the bulk electrolysis of 2 in a 0.25 M buffer solution ($\text{pH} 7.0$), and the charge significantly increased when the applied potential was set to be more negative. When the applied potential was -1.45 V versus Ag/AgCl , the maximum charge reached 1599 mC during 2 min of electrolysis in the presence of 2 (Fig. 7c), accompanied by a large amount of gas bubbles, which was confirmed as H_2 by gas chromatography. According to Fig. S9a, $\sim 9.918\text{ mL}$ of H_2 was produced over an electrolysis period of 1 h with a Faradaic efficiency of 98.68% for H_2 (Fig. S9-b). According to Eqs. (1) and (3), we also calculated the TOF for the catalyst as reaching a maximum of 909.58 moles of hydrogen per mole of catalyst per hour at an overpotential of 836.7 mV (Eq. (S4)). Remarkably, complex 2 is almost two times



Scheme 3. Proposed mechanism for proton reduction catalyzed by $[\text{LNi}]$.

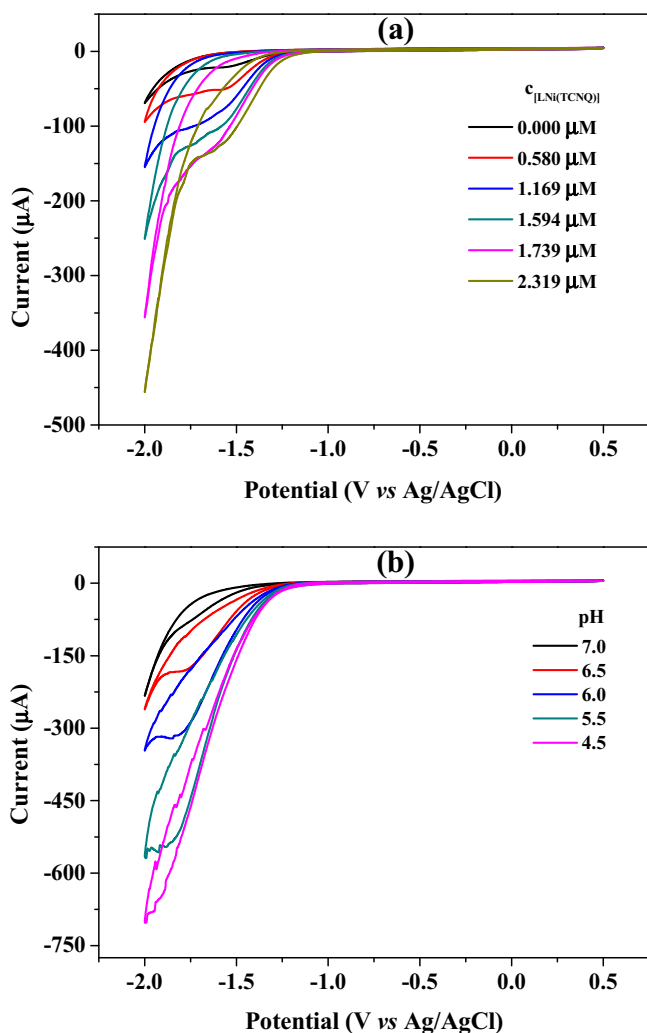


Fig. 6. (a) Cyclic voltammogram (CV) of complex **2** at different concentrations. (b) CVs of complex **2** (0.289 μM) at different pH values. Conditions: 0.25 M phosphate buffered solution (pH 7.0), glassy carbon working electrode (1 mm diameter), Pt wire counter electrode, Ag/AgCl reference electrode.

more effective than complex **1**. To the best of our knowledge, this value is significantly higher than some reported molecular catalysts based on nickel complexes for electrochemical hydrogen production from neutral water. For example, a similar nickel complex supported by 2,3-bis(2-hydroxybenzylideneimino)-2,3-butenedinitrile shows a TOF of 206 moles of H_2 per mole of catalyst per hour at an overpotential of 836.6 mV [8] and a dinickel complex exhibits a turnover number of 100 mol of H_2 per mole of catalyst at an overpotential of 820 mV [44]. This indicates that complex **2** is a highly active catalyst, probably because of its unique structure and properties: (1) $[\text{LNi}(\text{TCNQ})]$ (**2**) is soluble in water. (2) TCNQ^- , formed from **2** (Scheme 4) can stabilize a low oxidation state of nickel. This observation suggests that the presence of TCNQ is the key structural feature for eliciting proton and water reduction catalysis.

To prove that both complexes **1** and **2** act as homogeneous electrocatalysts, we measured the dependence of the catalytic current on the concentration of **1** or **2**. From Figs. 5a and 6a, the catalytic currents were indeed dependent on the concentrations of complexes **1** and **2**. Additionally, several other pieces of evidence suggest that these nickel complexes are homogeneous catalysts, as follows. (1) There is no evidence for a heterogeneous electrocatalytic deposit. For example, the electrode was rinsed with water

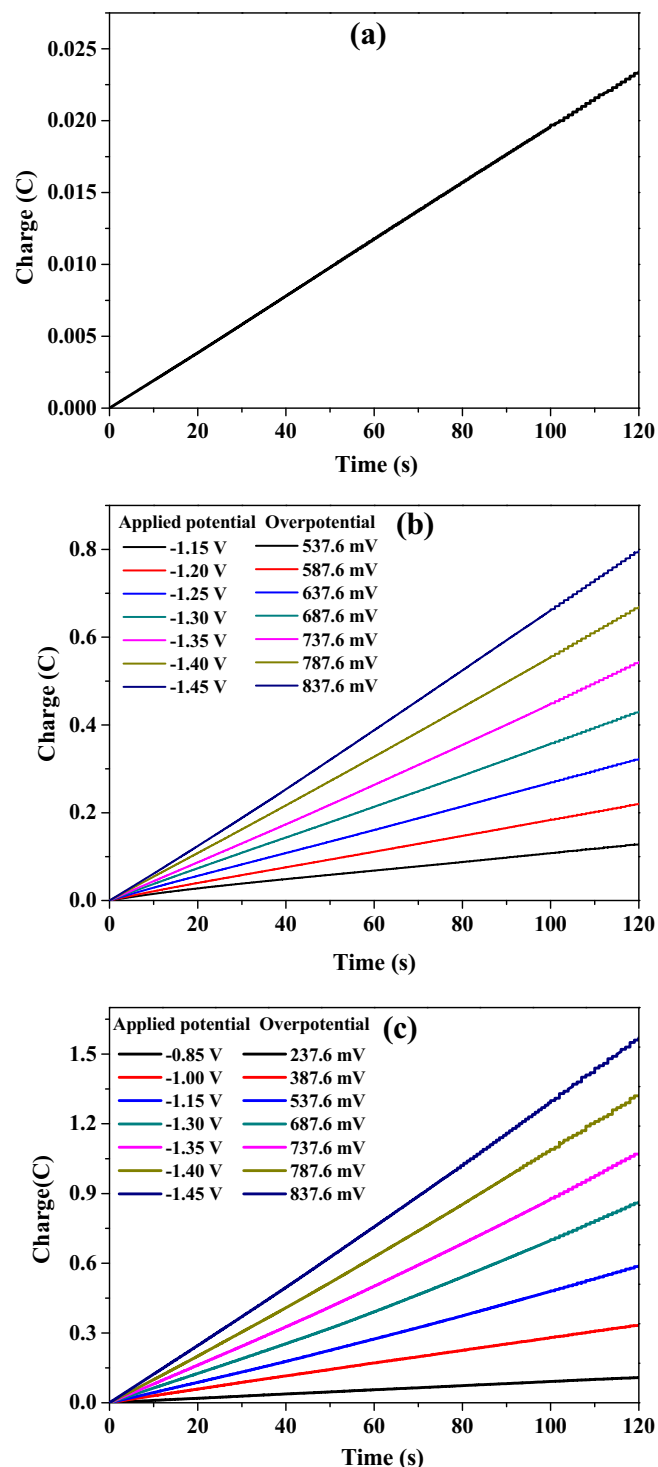
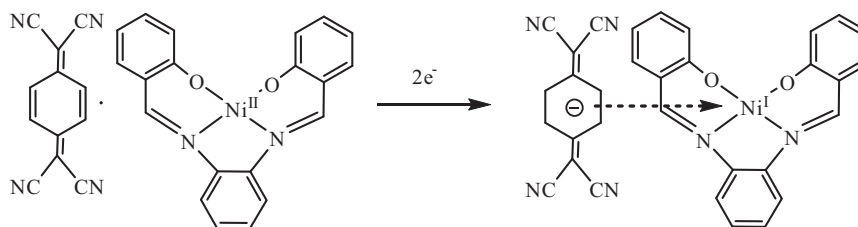


Fig. 7. (a) Charge build-up versus time from electrolysis of a 0.25 M buffer solution at -1.45 V versus Ag/AgCl. Charge build-up versus time from electrolysis of a 0.25 M buffer solution (pH 7.0) with 5.36 μM $[\text{LNi}]$ (**1**) (b), 5.36 μM $[\text{LNi}(\text{TCNQ})]$ (**2**) (c) under various applied potentials. All data have been deducted blank.

and electrolysis at -1.45 versus Ag/AgCl was run for an additional 2 min in 0.25 M phosphate buffer at pH 7.0 with no nickel complex present in solution. During this period, ca. 23 mC of charge was passed, a similar magnitude as observed for electrolyses conducted with freshly polished electrodes. (2) No discoloration of the electrodes was observed during cyclic voltammetry or bulk electrolysis.



Scheme 4. The formation of $[\text{LNi}^{\text{I}}\cdot\text{TCNQ}^-]$.

4. Conclusions

In this paper, we have described two nickel(II) complexes, that are easily obtained from the reactions of a simple nickel salt with a Schiff base ligand and which have been characterized by physico-chemical and spectroscopic methods. Both complexes can electrocatalyze hydrogen generation from acetic acid and aqueous buffer solution. Electrochemical studies show that the introduction of TCNQ into the nickel complex $[\text{LNi}]$ can improve the catalytic efficiency for hydrogen production, and this nickel complex, with a more positive $\text{Ni}^{\text{II/I}}$ redox potential, exhibits higher activity for hydrogen generation. Our ongoing efforts are focused on modifying the Schiff base ligand to give related water-soluble complexes with higher activity for further functional studies, with an emphasis on chemistry relevant to sustainable energy cycles.

Acknowledgements

This work was supported by the National Science Foundation of China (No. 20971045 and 21271073).

Appendix A. Supplementary data

CCDC 772098 contains the supplementary crystallographic data for this paper. These data can be obtained free of charge via <http://www.ccdc.cam.ac.uk/conts/retrieving.html>, or from the Cambridge Crystallographic Data Centre, 12 Union Road, Cambridge CB2 1EZ, UK; fax: (+44) 1223-336-033; or e-mail: deposit@ccdc.cam.ac.uk. Supplementary data associated with this article can be found, in the online version, at <http://dx.doi.org/10.1016/j.poly.2016.05.064>.

References

- [1] M.G. Walter, E.L. Warren, J.R. McKone, S.W. Boettcher, Q.X. Mi, E.A. Santori, N.S. Lewis, *Chem. Rev.* 110 (2010) 6446.
- [2] J.R. McKone, S.C. Marinescu, B.S. Brunshwig, J.R. Winkler, H.B. Gray, *Chem. Sci.* 5 (2014) 865.
- [3] X. Hu, B.S. Brunshwig, J.C. Peters, *J. Am. Chem. Soc.* 129 (2007) 8988.
- [4] H.M. Chen, C.K. Chen, R.S. Liu, L. Zhang, J.J. Zhang, D.P. Wilkinson, *Chem. Soc. Rev.* 41 (2012) 5654.
- [5] A. Thapper, S.R. Styring, G. Saracco, A.W. Rutherford, B. Robert, A. Magnuson, W. Lubitz, A. Llobet, P. Kurz, A. Holzwarth, S. Fiechter, H. de Groot, S. Campagna, A. Braun, H. Bercegol, V. Artero, *Green* 3 (2013) 43.
- [6] H.B. Gray, *Nat. Chem.* 1 (2009) 7.
- [7] M.L. Helm, M.P. Stewart, R.M. Bullock, M.R. DuBois, D.L. DuBois, *Science* 333 (2011) 863.
- [8] J.P. Cao, T. Fang, L.Z. Fu, L.L. Zhou, S.Z. Zhan, *Int. J. Hydrogen Energy* 39 (2014) 10980.
- [9] Y. Sun, J.P. Bigi, N.A. Piro, M.L. Tang, J.R. Long, C.J. Chang, *J. Am. Chem. Soc.* 133 (2011) 9212.
- [10] L.Z. Fu, L.L. Zhou, L.Z. Tang, Y.X. Zhang, S.Z. Zhan, *J. Power Sources* 280 (2015) 453.
- [11] B.D. Stubbert, J.C. Peters, H.B. Gray, *J. Am. Chem. Soc.* 133 (2011) 18070.
- [12] W.M. Singh, T. Baine, S. Kudo, S. Tian, X.A.N. Ma, H. Zhou, N.J. DeYonker, T.C. Pham, J.C. Bollinger, G.L. Baker, B. Yan, C.E. Webster, X. Zhao, *Angew. Chem. Int. Ed.* 51 (2012) 5941.
- [13] L. Tong, R. Zong, R.P. Thummel, *J. Am. Chem. Soc.* 136 (2014) 4881.
- [14] T. Fang, L.Z. Fu, L.L. Zhou, S.Z. Zhan, *Electrochim. Acta* 161 (2015) 388.
- [15] J.P. Cao, T. Fang, L.Z. Fu, L.L. Zhou, S.Z. Zhan, *Int. J. Hydrogen Energy* 39 (2014) 13972.
- [16] L.L. Zhou, T. Fang, J.P. Cao, Z. Zhu, X. Su, S.Z. Zhan, *J. Power Sources* 273 (2015) 298.
- [17] P. Zhang, M. Wang, Y. Yang, T. Yao, L. Sun, *Angew. Chem. Int. Ed.* 53 (2014) 13803.
- [18] J.P. Cao, T. Fang, L.L. Zhou, L.Z. Fu, S.Z. Zhan, *J. Power Sources* 272 (2014) 169.
- [19] J.P. Cao, T. Fang, L.L. Zhou, L.Z. Fu, S.Z. Zhan, *Electrochim. Acta* 147 (2014) 129.
- [20] C.C.L. McCrory, C. Uyeda, J.C. Peters, *J. Am. Chem. Soc.* 134 (2012) 3164.
- [21] D. Herebian, E. Bothe, E. Bill, T. Weyhermuller, K. Wieghardt, *J. Am. Chem. Soc.* 123 (2001) 10012.
- [22] R. Kato, H. Kobayashi, A. Kobayashi, *J. Am. Chem. Soc.* 111 (1989) 5224.
- [23] H. Zhao Jr., M.J. Bazile, J.R. Galan-Mascaros, K.R. Dunbar, *Angew. Chem. Int. Ed.* 42 (2003) 1015.
- [24] K. Nejati, Z. Rezvani, *New J. Chem.* 27 (2003) 1665.
- [25] G.M. Sheldrick, SADABS, Program for Empirical Absorption Correction of Area Detector Data, University of Göttingen, Göttingen, Germany, 1996.
- [26] G.M. Sheldrick, SHELXS 97, Program for Crystal Structure Refinement, University of Göttingen, Göttingen, Germany, 1997.
- [27] A. Nafady, A.M. Bond, A. Bilyk, A.R. Harris, A.I. Bhatt, A.P. O'Mullane, R.D. Marco, *J. Am. Chem. Soc.* 129 (2007) 2369.
- [28] S.L. Bartley, K.R. Dunbar, *Angew. Chem. Int. Ed.* 30 (1991) 448.
- [29] H. Miyasaka, C.S. Campos-Fernandez, R. Clerac, K.R. Dunbar, *Angew. Chem. Int. Ed.* 39 (2000) 3831.
- [30] M. María Ballesteros-Rivas, H. Zhao, A. Prosvirin, E.W. Reinheimer, R.A. Toscano, J. Valdés-Martínez, K.R. Dunbar, *Angew. Chem. Int. Ed.* 51 (2012) 5124.
- [31] S.A. O'Kane, R. Clérac, H. Zhao, X. Ouyang, J.P. Galán-Mascarós, R. Heintz, K.R. Dunbar, *J. Solid State Chem.* 152 (2000) 159.
- [32] T.S. Kistenmacher, J.E. Philips, D.O. Cowan, *Acta Crystallogr. Sec. B* 30 (1974) 763.
- [33] R.E. Long, R.A. Sparks, K.N. Trueblood, *Acta Crystallogr.* 18 (1965) 932.
- [34] L. Ballester, A. Gutiérrez, M.F. Perpiñán, M.T. Azcondo, A.E. Sánchez, U. Amaor, *Ann. Quim. Int. Ed.* 92 (1996) 275.
- [35] B. Olbrich-Deussner, W. Laim, G. Gross-Lannert, *Inorg. Chem.* 28 (1989) 3113.
- [36] L.R. Melby, R.J. Harder, W.R. Hertler, W. Mahler, R.E. Benson, W.E. Mochel, *J. Am. Chem. Soc.* 84 (1962) 3374.
- [37] G.A.N. Felton, R.S. Glass, D.L. Lichtenberger, D.H. Evans, *Inorg. Chem.* 45 (2006) 9181.
- [38] L. Lauterbach, J. Liu, M. Horch, P. Hummel, A. Schwarze, M. Haumann, K.A. Vincent, O. Lenz, I. Zebger, *Eur. J. Inorg. Chem.* 2011 (2011) 1067.
- [39] P.P. Liebgott, A.L. de Lacey, B.N.D. Burlat, L. Cournac, P. Richaud, M. Brugna, V. M. Fernandez, B. Guigliarelli, M. Rousset, C. Léger, S.B. Dementin, *J. Am. Chem. Soc.* 133 (2011) 986.
- [40] T.B. Rauchfuss, A.M. Royer, M. Salomone-Stagni, W. Meyer-Klaucke, *J. Am. Chem. Soc.* 132 (2010) 16997.
- [41] U.J. Kilgore, J.A.S. Roberts, D.H. Pool, A.M. Appel, M.P. Stewart, M.R. DuBois, W. G. Dougherty, W.S. Kassel, R.M. Bullock, D.L. DuBois, *J. Am. Chem. Soc.* 133 (2011) 5861.
- [42] C. Baffert, V. Artero, M. Fontecave, *Inorg. Chem.* 46 (2007) 1817.
- [43] H.I. Karunadasa, C.J. Chang, J.R. Long, *Nature* 464 (2010) 1329.
- [44] J.P. Collin, A. Jouaiti, J.P. Sauvage, *Inorg. Chem.* 27 (1988) 1986.